APPLICATION OF A FINITE-ELEMENT FORMULATION TO THE COLD COMPACTION OF METAL POWDERS

J.M. Prado, M.D. Riera, M.A. Miralles, G. Cugat

Departamento de Ciencia de los Materiales e Ingeniería Metalúrgica.
Universidad Politécnica de Catalunya.
E.T.S.E.I.B., Avda. Diagonal, 647. 08028-Barcelona. España

ABSTRACT

One of the main purposes of Powder-Forming is to make parts with a density distribution as uniform as possible. However, the most usual compacting technique, involving close-die compression, leads to nonuniform densification. Subsequent sintering does not modify significantly this result. Consequently, compacts present heterogeneous local deformation, what brings about residual stresses, which may cause fracture of the porous preform at ejection, nonuniform stress distribution in dies and nonhomogeneous mechanical properties of the porous compact and finished part.

In this work, a Cam Clay modified model of Plasticity has been employed to characterize the mechanical response of an iron powder. A Finite-Element formulation of ABAQUS, has provided the distribution of density, and also those of strain and stress in a cylindrical compact obtained by simple o double compression. We have also studied the influence of friction and geometry. Results of simulation are compared with those obtained on experimental procedures.

1. INTRODUCTION

Powder Metallurgy uses metal powder as its raw material and benefits from two characteristic features of granular materials: a) the possibility of transforming, by means of cold compression, a mass of powder into a porous aggregate with imposed shape and dimensions having a certain level of cohesion; b) the phenomenon of sintering among solid particles, which allows compacts to be consolidated by heating below melting temperature and giving place to a coherent metallurgical structure.

The research effort of powder metallurgical industries has been mainly centered on the sintering stage of production. But, current techniques of powder pressing, by means of closed dies, usually produce heterogeneous densification which is hardly changed during the posterior sintering. Thus, compacts show unhomogeneous local deformation, giving place to residual stresses which can cause their fracture during part ejection, non-uniform stress distribution on the dies and, also, heterogeneous properties of both the porous aggregate and finished part. So, the knowledge of the mechanisms acting during the compaction stage becomes of primary importance in order to obtain uniform density distribution in finished parts.

It has been known for long time that granular materials and, among them, metal powders, show several different densification mechanisms during compression [Shapiro, 1947]. Firstly, for low pressures, occurs particle sliding. Under this mechanism, particles rearrange in a way that has been compared with the compact packing of crystalline structures [Artz, 1982]. At higher pressures, takes place the plastic deformation of particles through their contact areas. At even higher pressures, the flow resistance of the material increases more rapidly due to the strain and geometrical hardenings (the latter

one is caused by the progressive increment of the contact areas between particles). For relative densities of the compact close to the bulk (R=1), its compressibility decreases drastically due to the already mentioned effects and also to the air and lubricant entrapped inside the pores.

The aim of this work has been to find a model able to represent all these stages of compaction, but making special emphasis on the two first of them, as they are the only ones usually acting during an industrial compression.

2. CONSTITUTIVE MODEL

Most of the frictionals materials undergo, from very low pressures, inelastic deformation, even for hydrostatic states of stress. Furthermore, during subsequent flow, the material hardens, in a way that, when the tension point moves beyond the actual yield locus, a new locus is established. This behaviour has been represented by Roscoe et al. [Roscoe, 1952] by means of a series of yield surfaces (caps) previous to reaching the critical state which separates the zones of consolidation and failure [Desai, 1984]. Figure 1 shows, in the "hydrostatic pressure-deviator stress" space, the CAM model, which incorporates the idea of critical state [Drucker-Prager, 1952] by means of a fixed yield surface and the continuous flow of the material with a series of additional yield surfaces. One of the characteristics of this combination of surfaces is that, in their intersection, representing the point of critical state, the tangent to the cap is horizontal. Hence, the plastic flow at the critical state is at constant volume meaning that the rule of associated flow is fulfilled. The stress-strain behaviour can be studied using the space "mean pressure logarithm-void ratio", by measuring the total change in the void ratio during a cycle of loading-unloading. The

result, shown in figure 2, comprises two straight lines, one ABC of slope λ, corresponding to the plastic modulus of the material; and another, BD, of elastic recovery which slope is the logarithmic modulus, k. The expression for the components of volumetric deformation can be deduced from the equations of those straight lines:

$$d\varepsilon_v = -\frac{de}{1+e_o} = \frac{\lambda}{1+e_o}\frac{dp}{p} \qquad (1)$$

$$d\varepsilon^e_v = -\frac{de^e}{1+e} = \frac{k}{1+e}\frac{dp}{p} \qquad (2)$$

$$d\varepsilon^p_v = \frac{de^p}{1+e} = \frac{\lambda-k}{1+e}\left(\frac{dp}{p}+\frac{d\eta}{\psi+\eta}\right) \qquad (3)$$

where η is the ratio between the shear and hydrostatic components, ψ is the slope of the yield curve on any point (p, q), and, in agreement with the normality condition:

$$\psi = -\frac{dq}{dp} = \frac{d\varepsilon^p_s}{d\varepsilon^p_v} \qquad (4)$$

because the vector of incremental plastic strain is normal to the yield surface on any point. In this model:

$$d\varepsilon^p_s / d\varepsilon^p_v = 2\eta/(M^2-\eta^2) \qquad (5)$$

From all these expressions, the equation representing the yield locus for the CAM model can be derived; namely:

$$f = M^2p^2 - M^2p_o p + q^2 = 0 \qquad (6)$$

corresponding to the equation of an ellipse on the plane "p-q". From the normality condition for plastic deformations, which can be expressed as:

$$d\varepsilon^{p}_{ij}=\bar{\lambda}.\partial g/\partial\sigma_{ij} \qquad (7)$$

and the associated flow rule (g=f), the following constitutive equation can be deduced:

$$d\sigma_{ij}=[C_{ijkl}-(C_{ijkl}A_{kl}B_{mn}C_{mnrs})/(B_{mn}C_{mnrs}A_{rs}-(\partial F/\partial\varepsilon^{p}_{v})A_{ii})]d\varepsilon_{rs} \qquad (8)$$

where C_{ijkl} represents the elastic matrix; A_{ij}, is $\partial g/\partial\sigma_{ij}$, and B_{ij}, is $\partial f/\partial\sigma_{ij}$.

3. MODEL PARAMETERS DETERMINATION

In order to be able to implement the model explained, the material parameters λ, k, M and p_o, need to be known. It will be now shown how this can be done, in a relatively simple way for an iron powder.

The material used in this work has been an iron powder elaborated by Höganäs (ASC 100.29), of spherical shape and high compressibility. The "compressibility curve", relating the applied axial pressure and the relative density, has been determined by pressing the material in a cylindrical die and is shown in Fig. 3.

The radial component of stress during compression can be deduced from the axial pressure by means of the expression derived by Pleney and Meyer [Pleney and Meyer, 1978]:

$$\sigma_r=(\nu_p/(1+\nu_p))(\sigma_1-Y_R) \qquad (9)$$

where the plastic Poisson's coefficient ν_p and the elastic limit for the porous preform depend on the porosity in a way given by Pleney and Meyer [Pleney and Meyer, 1978]:

$$\nu_p=0.5(1-1.6n) \tag{10}$$

$$Y_R=Y_b(1-3n) \tag{11}$$

here, n is the porosity of the preform and Y_b is the elastic limit of bulk metal (taken as 140 MPa for plain iron). Due to the axial symmetry of the system, the circumferential component of stress coincides with the radial one. The curve "hydrostatic pressure vs. shear stress" can now be represented and is shown in Fig. 4. It can be assumed that the initial condition of the metal powder inside the die, before any pressure is applied, corresponds to a "critical state"; during subsequent compaction, the material consolidates and folows a path in the p-q space which crosses the hardening caps and is more and more separated from the line of "critical states". Therefore, the straight line tangent at the origin to the p-q compaction path should coincide with the line of critical states separating the regions of consolidation and that of failure (material swelling) and its slope M is one of the parameters of this model.

Once M is known it is now possible to determine the ellipses corresponding to each of the consolidated states reached by the powder during the compression path.

In equation (6), the only unknown parameter is now p_o, which can be found for each of the points in the compression path and, consequently, the succesives hardening caps. These have been represented in Fig. 5. The determination of a_o, intersection between the caps and the line of critical state is now inmediate.

Finally, the "stress-strain" behaviour has been characterized representing the values of a_o as a function of the void ratio, e. Fig. 6 shows the relation "ln a_o-e" for the iron powder under study and it can be seen the existance of two straight lines, corresponding to each of the two different mechanisms which are acting during compaction. The slope of each line gives the parameter λ corresponding to each of the stages of compaction. From this curve, the densities which define the extension of the compression path dominated by one of the consolidation mechanisms, can be determinated.

The elastic component of volume deformation has been introduced in this model by supossing that it is proportional to the logaritm of the applied pressure in the following way:

$$\frac{k}{1+e_o}\ln[(p_o+p_t)/(p+p_t)]=J^{el}-1 \qquad (12)$$

To implement the elastic part of the model, the parameter k, the logarithmic modulus, and p_t, uniaxial tensil elastic limit, should be known. The value of k is easily determined by means of unloadings during the compression path (Fig. 2), while p_t is taken equal to zero because effective tensile resistance is considered to be reached only by posterior sintering.

Density distributions in compacted specimens has been experimentally determined using a method based on the existance of a correlation between hardness and density in a porous material. Therefore, Vickers hardness distributions (1 Kg) were found on compacted samples (H/D=1) which previously underwent a thermal annealing (1100 C, 20 min)to eliminate the plastic hardening contribution. By means of a calibration curve it is now possible to draw the density distributions as it is shown in Fig. 7 for a sample with a relative

density of R=0.825.

4. FINITE ELEMENTS SIMULATION

The elastic and plastic models have been implemented in the Finite Element Program ABAQUS, version 4.8, by using the POROUS ELASTIC and CLAY PLASTICITY options, respectively [ABAQUS, 1989].

The general case used to validate the constitutive model, has been the die compaction of a cylinder in which the ratio between high and diameter after compaction is 1 (H/D=1). Then, the FE model is axisymmetric and includes only the top half of the specimen, since the middle plane of the cylinder is a plane of symmetry. The FE mesh is composed by 144 elements of type CAX with a total of 169 nodes. The die and punch are assumed rigids and they are modelled with interface elements of type IRS to the outer surface of the cylinder. Boundary conditions are used in order to impose to the nodes of the rigid surface corresponding to the punch a downwards displacement, of given value and constant velocity, representing the axial compression. All the specimen top surface nodes, unless those of the upper corner, have the same boundary conditions of those of the punch, because they must remain always in contact.

The study of the process has been carried out as a static analysis, non-linear, with convergence control to ensure that non-linear equilibrium is satisfied. As numerical solving technique, the Newton standard method has been used.

The compaction simulation has been applied from an initial relative density of R= 0.4000 up to a final one of R= 0.8752, subdivided in two individual programs for each stage of compaction.

Friction between the iron powder and the walls of the die and punch is modelled in the ABAQUS program by using the Coulomb law. A friction coefficient of 0.3 has been taken for the general case, and of 0.1 and 0.5 to study the influence of friction on the density distribution.

The effect of geometry has been considered by changing the relation between height and diameter of the cylinder from 1 (general case) to 0.5.

The effect of the type compaction process has been studied by modelling double compression. In this case, the compression due to the motion of a lower punch has been added.

5. RESULTS AND DISCUSSION

Fig. 8 shows the density distribution for the general case (H/D=1; μ=0.3 and single compression). The greatest density values are obtained on the right upper corner, where the powder is directly in contact with die and punch. Moving away from this region, there is a gradual decrease of density with a minimum value on the left lower corner, where the trasmitted pressure and powder motion reach a lower value. Inside the compact, there is a clear tendency to a stratification in layers of decreasing density. It must be also pointed out that the gradient of relative density during the first stage of compaction (0.04) is smaller than the one of the second stage (0.09), due to the different mechanisms of deformation and densification.

The effect of geometry is mainly characterized by a progressive increment of the relative density gradient when the shape ratio, H/D, increases. It is patent from the results presented in Fig. 9, and in

the Table I, how the effect of friction is enhanced when the shape ratio increases.

The effect of friction is reflected in Table II and in Figs. 10 and 11, which corresponds to the compression of a compact with H/D=1 and different friction coefficients.

The results for the process of double compression, for H/D=1 and μ=0.3, are shown in Fig. 12. The relative density gradient is now smaller, and there is also the ocurrence of a "neutral zone" of minimum density at the equatorial plane of the specimen with symmetric density distribution at each side of it.

6. CONCLUSIONS

The model applied and the results obtained permit to conclude that the mechanisms envolved in each stage do not exclude each other, although one of them predominates. It is even possible to find regions where particles are mainly deforming plastically when in a nearby region they are still at the sliding stage.

The results of these work permit also to conclude that CAM plasticity model reproduces accurately the existance of the different mechanisms acting during the compaction of metal powders. Furthermore, experimental results are in good agreement with those predicted by the model.

Finally, the Finite Elements method applied to the resolution of the CAM model is a useful and reliable tool for the determination of the density distributions of porous compacts.

Acknowledgments

The authors wish to thank "Principia" for its help throughout this work.

7. REFERENCES

ABAQUS USER'S MANUAL. Version 4.8. HKS, Inc. (1989).

ARTZ, E. Acta Metallurgica. Vol. 30, pg. 1883 (1982).

DESAI, C.S.; SIRIWARDANE, H.J. "Constitutive Laws for Engineering Materials". Ed. Prentice-Hall, Inc. Englewood Cliffs (1984).

DRUCKER, D.C.; PRAGER, W. Quart Appl. Math. Vol. 10, No. 2, pg. 157 (1952).

PLENEY, L. MEYER, R. P/M SEMP. Estocolmo (1978).

ROSCOE, K.H. et al. Geotechnique. Vol. 8, pg. 22 (1958).

SHAPIRO, I.; KOLTHOFF, I.M. Journal of Physics Colloid Chem. Vol. 51, pg. 483 (1947).

H/D	R_{max}	R_{min}
0.5	0.882	0.866
1	0.930	0.849

Table I.- Effect of geometry.

μ	R_{max}	R_{min}
0.1	0.900	0.860
0.3	0.930	0.849
0.5	0.960	0.840

Table II.- Effect of friction.

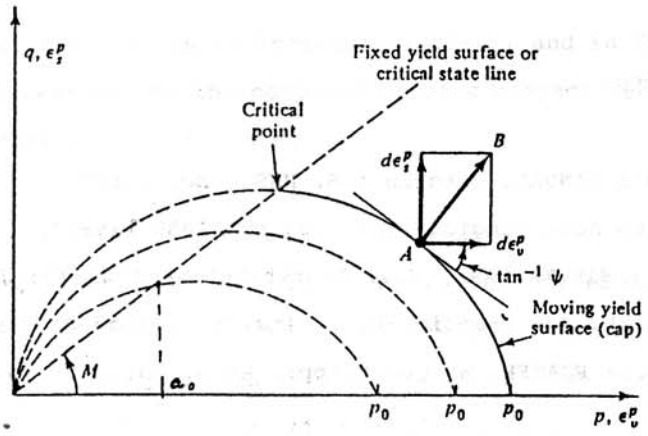

Fig. 1.- CAM model.

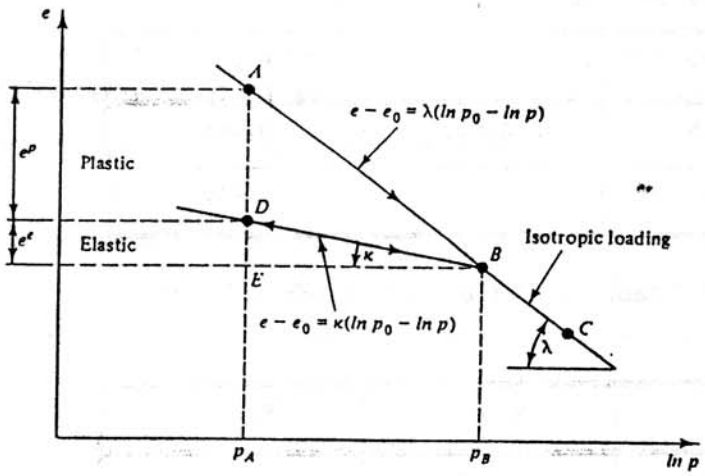

Fig. 2.- Stress-strain behaviour.

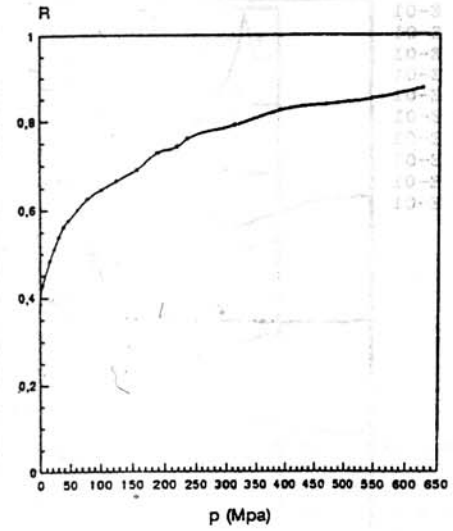

Fig. 3.- Compressibility curve.

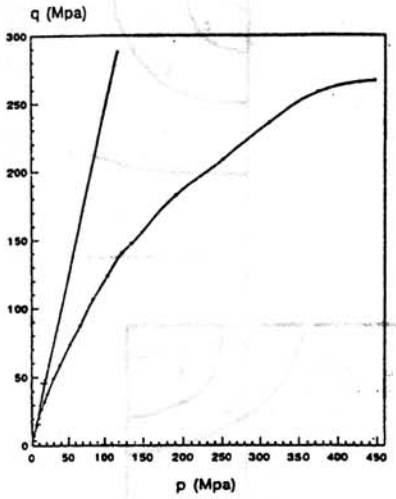

Fig. 4.- "p-q" curve.

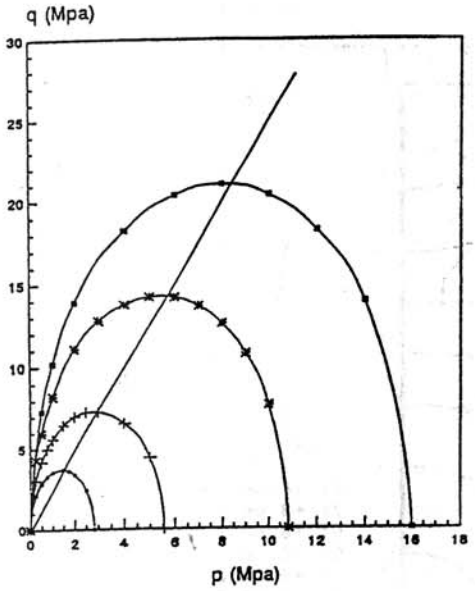

Fig. 5.- Yield surfaces.

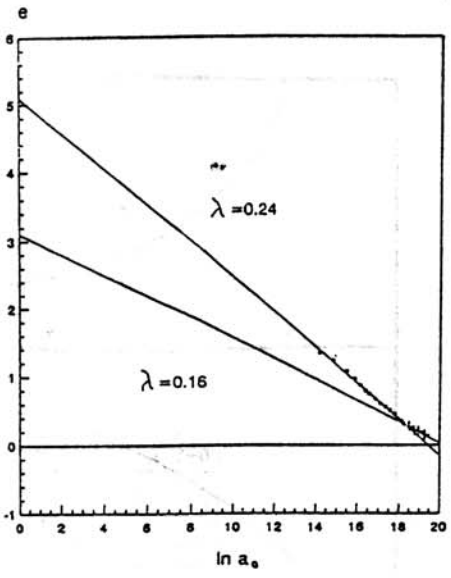

Fig. 6.- Relation "ln a_o-e".

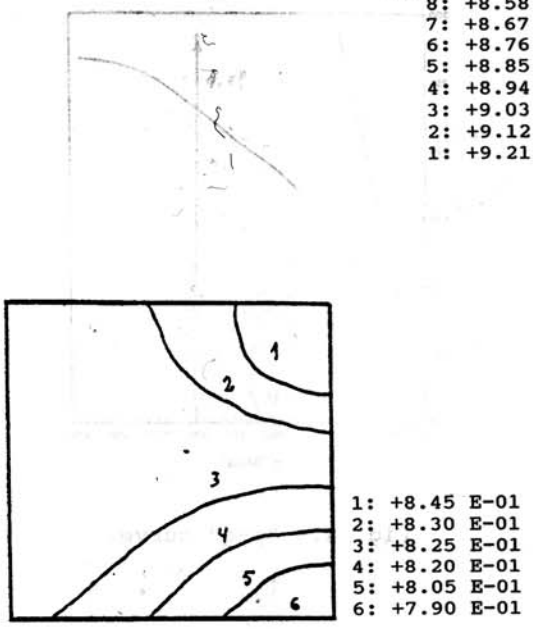

Fig. 7.- Experimental density distributions.

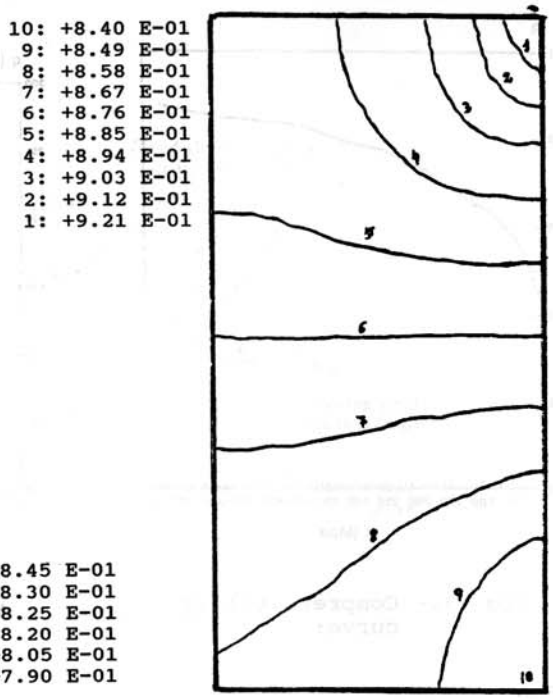

Fig. 8.- Density distribution H/D=1; μ=0.3; single compression.

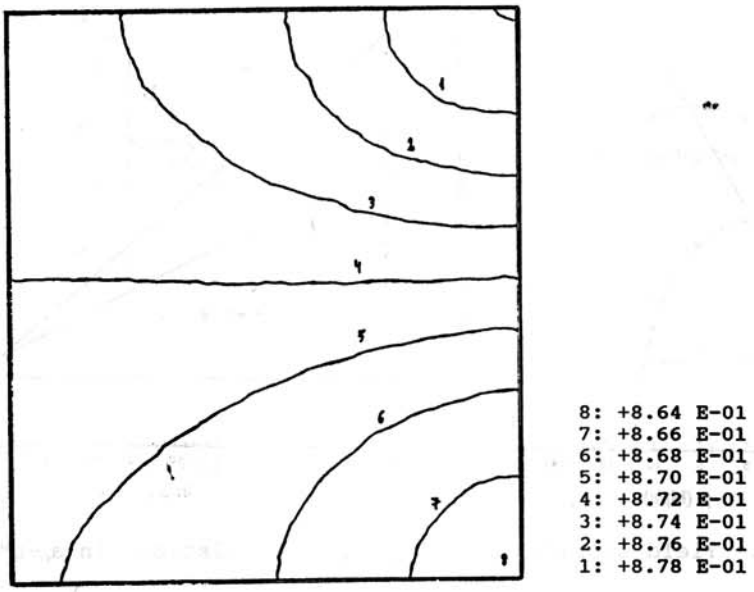

Fig. 9.- Density distributions H/D=0.5; μ=0.3; sing. comp.

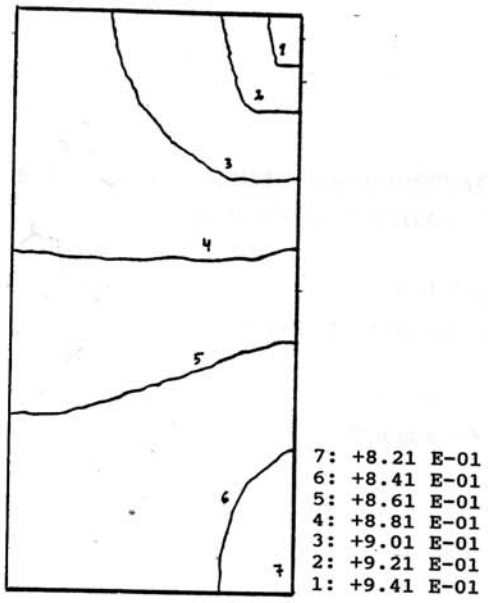

Fig. 10.- Density distributions. H/D=1; μ=0.1 single compression.

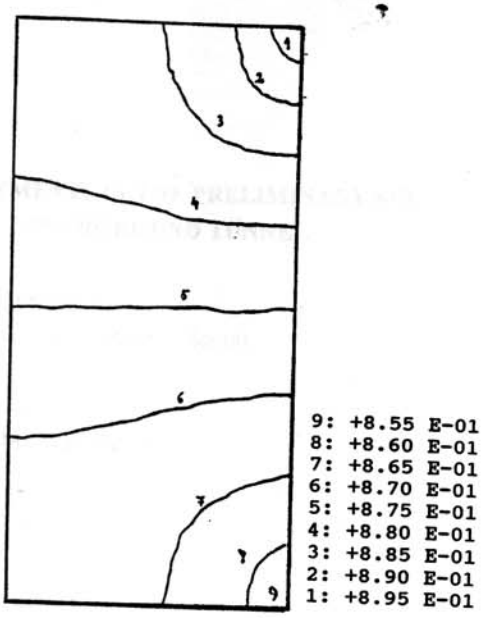

Fig. 11.- Density distributions. H/D=1; μ= 0.5 single compression.

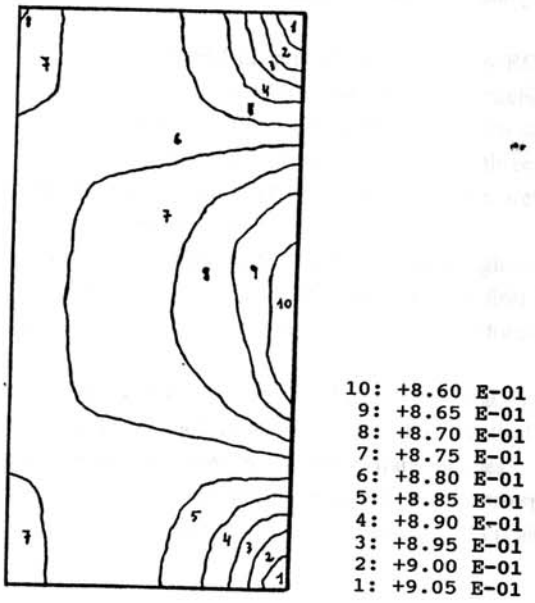

Fig. 12.- Density distributions H/D=1; μ=0.3; double compression.